IOPscience iopscience.iop.org

Home Search Collections Journals About Contact us My IOPscience

Viable route towards large-area 2D MoS_2 using magnetron sputtering

This content has been downloaded from IOPscience. Please scroll down to see the full text.

2017 2D Mater. 4 021002

(http://iopscience.iop.org/2053-1583/4/2/021002)

View the table of contents for this issue, or go to the journal homepage for more

Download details:
This content was downloaded by: dmazumdar
IP Address: 131.230.51.58
This content was downloaded on 11/01/2017 at 15:45

Please note that terms and conditions apply.

2D Materials

RECEIVED
2 June 2016

REVISED
26 November 2016

ACCEPTED FOR PUBLICATION
8 December 2016

PUBLISHED
11 January 2017

LETTER

Viable route towards large-area 2D MoS_2 using magnetron sputtering

Hassana Samassekou[1], Asma Alkabsh[1], Milinda Wasala[1], Miller Eaton[1], Aaron Walber[1], Andrew Walker[1], Olli Pitkänen[2], Krisztian Kordas[2], Saikat Talapatra[1], Thushari Jayasekera[1] and Dipanjan Mazumdar[1]

[1] Department of Physics, Southern Illinois University, Carbondale, IL 62901, USA
[2] Faculty of Information Technology and Electrical Engineering, Microelectronics Research Unit, University of Oulu, Oulu, Finland

E-mail: dmazumdar@siu.edu

Keywords: transition metal dichalcogenides, thin films, MoS_2, 2D materials

Supplementary material for this article is available online

Abstract

Structural, interfacial, optical, and transport properties of large-area MoS_2 ultra-thin films on BN-buffered silicon substrates fabricated using magnetron sputtering are investigated. A relatively simple growth strategy is demonstrated here that simultaneously promotes superior interfacial and bulk MoS_2 properties. Few layers of MoS_2 are established using x-ray reflectivity, diffraction, ellipsometry, and Raman spectroscopy measurements. Layer-specific modeling of optical constants show very good agreement with first-principles calculations. Conductivity measurements reveal that few-layer MoS_2 films are more conducting than many-layer films. Photo-conductivity measurements reveal that the sputter deposited MoS_2 films compare favorably with other large-area methods. Our work illustrates that sputtering is a viable route for large-area device applications using transition metal dichalcogenides.

1. Introduction

During the last decade, layered materials have caused a paradigm-shift in our understanding of the fundamental properties of nanomaterials and opened up new technological possibilities. The discovery of single-layer graphene [1, 2] and transition metal dichalcogenides (TMDs) [3, 4], initially through mechanical exfoliation, have sparked a series of high profile discoveries that impact numerous electronic and optoelectronic areas [5–7], and opened up potentially new areas [8, 9].

TMDs offer many advantages because of their unique and tunable electronic properties. MoS_2, one of the most investigated TMD in recent years, changes from an indirect (1.3 eV) to a direct (1.8 eV) gap system as it is shrunk to a monolayer [10]. Other TMDs such as $MoSe_2$ [11], WS_2, WSe_2 [12] show similar properties. It is not a surprise that such materials have demonstrated many high performance devices using single or bilayer MoS_2 such as field effect transistor [13], photodetector [14, 15], memory [16], integrated circuit [17] to name a few.

Growth of large-area MoS_2 has been demonstrated primarily using chemical vapor deposition (CVD) technique [7, 18–20]. Vacuum-based methods such as pulsed laser deposition (PLD) [21–23], and magnetron sputtering [24] have also displayed promise. Also many applications necessitates that the TMDs be compatible with a wide variety of substrates, apart from large-area growth. Previous studies have shown that optical properties of MoS_2 and other TMDs are significantly influenced by the underlying substrate [25–27]. In particular, in a very recent study [27], using mechanically exfoliated MoS_2 and h-BN flakes, it was shown that an atomically thin buffer layer of h-BN protects a range of key properties of monolayer MoS_2.

Motivated by such developments, we examine the properties of large-area MoS_2 thin films down to approximately four layers deposited on thin amorphous boron nitride buffered silicon substrates grown using RF magnetron sputtering. The focus of this work is to investigate simultaneously interface and bulk structural properties leveraging primarily upon established large-area thin-film characterization techniques such as x-ray reflectivity and diffraction. Spectroscopic ellipsometry, transport, and first-principles calculations are employed to investigate the electronic properties of the large-area films. Previously we have demonstrated growth of many-layer MoS_2 films with well-defined Raman peaks and photo-responsivity [28]. Here we extend and deepen the scope of the previi-

© 2017 IOP Publishing Ltd

ous work. What distinguishes our work is that we have developed a relatively simple strategy to grow high quality few-layer MoS_2 that mainly comprises of post-deposition annealing after a low temperature growth. Combined with ellipsometry and Raman characterization we confirm that it is possible to deposit highly uniform, large area few layers (~3–4 layers) of MoS_2. Transport measurements reveal that the conductivity of few-layer films is higher that the many-layer films deposited with our method. We also show that electrical conductivity of devices fabricated using these deposited films show very consistent results, indicating that the process presented here can lead to large area, few layer TMD layers with reliable physical properties.

2. Methods

Boron nitride (BN) and MoS_2 layers were grown using commercially available stoichiometric targets and RF sputtered in a high vacuum magnetron sputter system (base pressure 4×10^{-9} Torr) under different deposition conditions. Particularly, growth temperature (room temperature to 400 °C), and post-deposition annealing temperature (300–750 °C) were varied. Deposition of amorphous BN was carried out in a 1:10 N_2/Ar mixture to produce stoichiometric films. Based on our prior result we concluded that high temperature growth (300 °C or over) could lead to unwanted interfacial layers and disordered MoS_2 [1]. As we show here, an appropriate post-deposition annealing treatment following a low temperature growth (best at room temperature) leads to sharp interfaces and crystalline MoS_2.

X-ray reflectivity (XRR) and x-ray diffraction (XRD) patterns were evaluated using a high resolution Rigaku Smart Lab x-ray diffractometer equipped with a channel-cut Ge (2 2 0) crystal to produce a highly monochromatic K-alpha radiation. XRR data was analyzed using GenX software [29] that implements the Parratt formalism of multi-layers [30]. Optical constants such as the refractive index (n, k) were measured in the 0.8–4.2 eV range using variable angle spectroscopic ellipsometry (J A Wollam WVASE and M2000V) and modeled using the VWASE32 software to extract layer-specific properties. Raman measurements were performed with Nanophoton Raman-11 spectrometer using a 532 nm laser. Both large-area and single-spot measurements were performed to verify the properties of MoS_2 films.

3. Results and discussion

In figure 1(a) we show the optical image of an optimal 20 nm MoS_2 film deposited on BN-buffered silicon substrate. In comparison to a bare substrate, the color contrast is distinct. The thickness homogeneity of the sample is primarily limited by the size of sputtering target (2 inch diameter in our sputtering system), and we expect our films to be very uniform over 1×1 inch area. In figure 1(b), we show a large atomic force microscopy (AFM) scan of a 10–20 nm (many-layer) MoS_2 film. As evident from the nearly uniform color, and also from the surface profile data (figure 1(c)), our samples are extremely smooth with a root-mean-square roughness of less than 0.25 nm. Thinner, few-layer samples are smoother. This is typically of a 3D growth mode that is expected for the low temperature synthesis employed here (see figure S3 in supplementary (stacks.iop.org/TDM/4/021002/mmedia)).

In figure 2(a), we show the XRR data for a many-layer MoS_2 film grown on sputtered a-BN at room temperature (black line, labeled 'RT') and after a 2 h–485 °C annealing treatment (red line, labeled '485 °C'). Clear fringes are observed in both cases up to $2\theta = 4°$. This is a qualitative feature of sharp interfaces over large area. However to proceed further, a quantitative analysis is needed [29, 30]. Various relevant information can be extracted from XRR data such as thickness, large-area roughness, and density values of each individual layer; and, the values for both conditions are outlined in table S1. The fit data for the annealed sample is shown in figure 2(b) along with the extracted thickness values for the different layers in the inset. Let us discuss the XRR features in some detail. The critical angle, θ_c, the angle at which x-rays start to penetrate the sample is related to the density of the underlying layer(s). Higher θ_c indicates higher density which is realized for the annealed (485 °C) sample as shown in the inset of figure 2. The extracted MoS_2 density (0.018 g cm^{-3}) after annealing is very close to the bulk value (0.019 g cm^{-3}). Our analysis also finds a large 7 nm (35%) change in MoS_2 thickness upon annealing that can be qualitatively inferred from the changing periodicity of the thickness oscillations. This is suggestive of major structural changes and consistent with crystallization of the MoS_2 layer, as also evidenced in our XRD, Raman and optics data (discussed later). No additional interfacial layer was required to obtain a good fit apart from a native SiO_2 layer. This is in contrast to a high temperature growth method that we have reported earlier [28]. Therefore, we can conclude that a low temperature growth with appropriate post-deposition annealing promotes desirable features for MoS_2.

In figure 3(a), we show the θ–2θ scan for a thick, 40 nm MoS_2 film. Clear diffraction peaks are obtained for silicon substrate (labeled as "Sub") and the (0 0 0 2) MoS_2 layer as indicated. We have verified that the low angle peak is from MoS_2 and not BN by measuring separate BN thin film samples. The effect of annealing temperature on the inter-planar distance of MoS_2 is shown in figure 3(b). The lattice parameter gradually decreases at higher temperatures which is consistent with the expected strain-relaxation effect, but still somewhat larger than the bulk value (dashed green line). The peak intensity also increases substantially with increase in temperature (figure S1), implying better crystal quality with annealing. However, beyond 485 °C, multiple phases appear in the XRD dada (figure S1) implying that MoS_2 is chemically unstable beyond a certain high temperature.

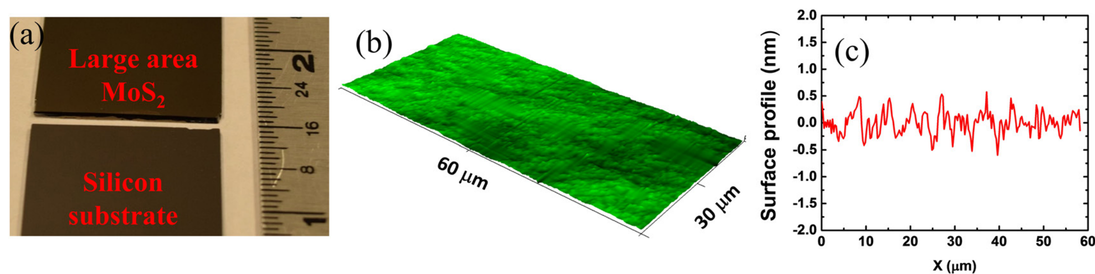

Figure 1. (a) Optical image of an optimized large-area 20 nm MoS_2 sample grown on BN-buffered silicon substrate using sputter deposition method. A bare silicon substrate is also shown in comparison to highlight the color contrast. (b) A 60 × 30 μm AFM scan of a 20 nm MoS_2 film showing smooth surface morphology. (c) Typical surface profile (line scan) of the AFM data shown in (b). The average peak-to valley variation is less than 1 nm.

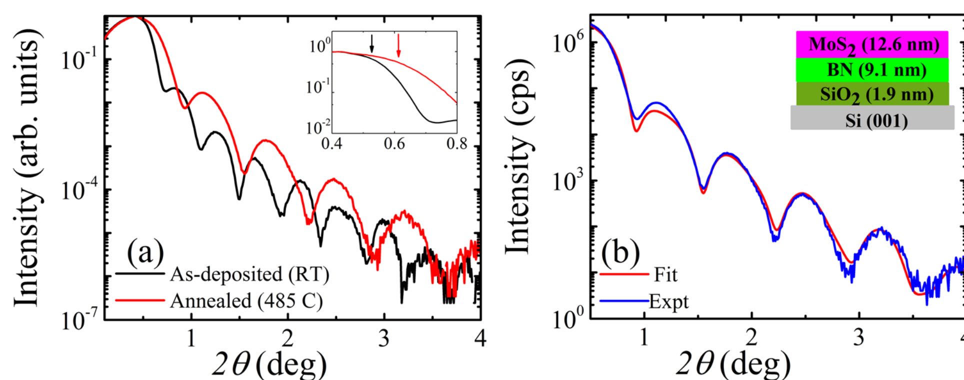

Figure 2. (a) XRR curve of the BN-MoS_2 heterostructure grown on Si (0 0 1) substrate before (black), and after (red) annealing. Inset of figure 1(a) shows the change in critical density in the two cases. (b) The optimally annealed sample (485 °C) is fitted to obtain the layer-specific thickness, roughness, and density. The thickness values of the layers are listed in the inset schematic diagram.

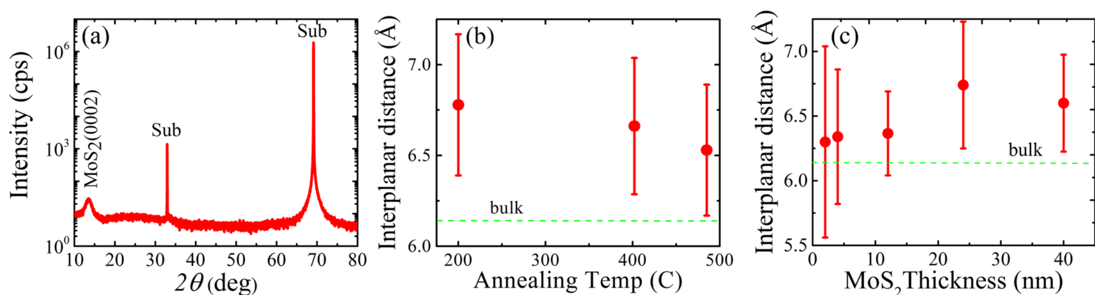

Figure 3. (a) XRD pattern of many-layer MoS_2 on BN-buffered (0 0 1)-oriented Si substrate. (b) Variation of distance between MoS_2 layer as a function of annealing temperature. (c) The measured out-of-plane interplanar distance versus film thickness for optimally annealed samples.

Based on our XRR thickness calibration values (and ellipsometry), we fabricated a series of MoS_2 samples down to approximately 2.5 nm. The evolution of the interplanar distance as a function of thickness is plotted in figure 3(c) for the samples shown in figure S2 and table S2. Our result indicates that the MoS_2 layer sharply transitions to bulk-like lattice parameter values for less than 10 nm thickness. This could imply that thicker (>10 nm) films have a high degree of disorder in the form of defects and vacancies, a finding that is also supported by Raman measurements, but contrary to our initial expectation. From now on, we shall primarily discuss the properties of the few layer MoS_2 sample (labeled FL-MoS_2) of thickness ~2.5 nm that corresponds to 4 layers.

We have performed additional characterization using Raman spectroscopy in order to verify thickness and properties of our MoS_2 films (figure 4). Raman spectroscopy is a strong tool, which is widely used in order to determine the vibrational modes of layered chalchogenides. The values obtained for various vibrational modes are akin to the layer numbers and hence can be used to determine the number of layers. For example, in case of MoS_2 two predominant vibrational modes, one at ~407 cm^{-1} another at ~383 cm^{-1} belong to the out of plane A_{1g} mode and the in plane E^1_{2g} mode

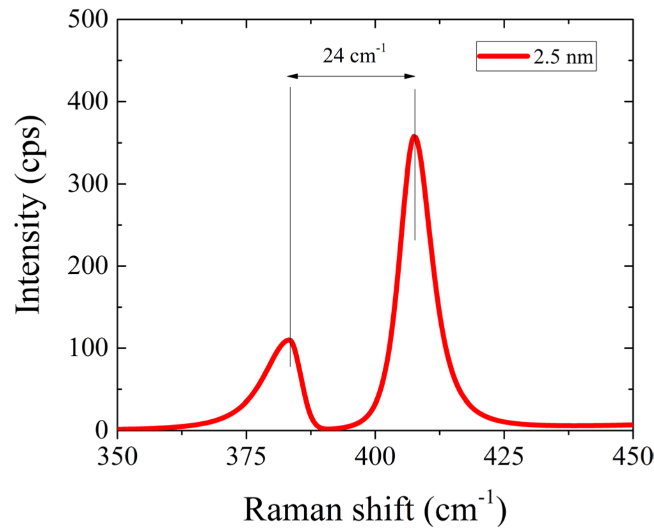

Figure 4. Raman spectra of the FL-MoS_2 sample (~2.5 nm) showing the characteristic E^1_{2g} and A_{1g} vibrational modes of MoS_2.

respectively. The frequency difference ($\Delta\omega$) between the A_{1g} and the E^1_{2g} modes is a good indicator of number of layers present in MoS_2. Typically $\Delta\omega \sim 26\,cm^{-1}$ corresponds to bulk MoS_2, whereas $\Delta\omega \sim 18$–$19\,cm^{-1}$ corresponds to monolayer of MoS_2. We have consistently obtained a value of $\Delta\omega \sim 24\,cm^{-1}$ for FL-MoS_2 samples as shown in figure 4 indicating that they are indeed closer to 4 layers. We have also seen that $\Delta\omega$ values slowly approaches to ~$26\,cm^{-1}$ for thick samples consistent with our past results [28].

Another indicator of film quality is the full width at half maxima (FWHM) of the observed vibration modes. FMHM values for the sputtered FL-MoS_2 film is compared with literature values in table S3. Typical values for exfoliated MoS_2 and CVD grown films is ~2–6 cm^{-1} for the E^1_{2g} mode, and 4–6 cm^{-1} for the A_{1g} mode. In comparison, our 4-layer films have slightly higher values of 8.5 and 7.4 cm^{-1} respectively. Apart from vacancy induced disorder, roughness from the BN underlayer could also contribute to the observed FWHM. This will be tested in future studies. Another observation is that the many-layer films show much higher FWHM (10–15 cm^{-1}) that is consistent with our earlier inference that thicker films (>10 nm) are more disordered compared to few-layer films. This also has important implications on the transport properties of few-layer films as discussed later.

To check the robustness of the Raman modes with respect to device processing, we have characterized the deposited films before and after a photo-lithography process. The consistency of the Raman data obtained from multiple areas of many-layer sample (see figure S4) on the films before and after photo lithography process indicates the robustness of these films. From the measurements it is clear that the photolithography process does not destroy the integrity of the deposited films. Similar Raman results were also obtained from the few-layer MoS_2 samples (data not shown).

The optical properties of sputter-grown MoS_2 samples of various thickness were investigated using spectroscopic elipsometry (SE) in the 0.8–4.2 eV range. Ellipsometry is a popular, non-destructive technique that can provide thickness and optical constant values of thin films by measuring the ratio of p- and s- reflectance. This ratio is depicted by a complex number ($\tilde{\rho}$) given by

$$\tilde{\rho} = \frac{\widetilde{R_p}}{\widetilde{R_s}} = \tan\Psi e^{i\Delta} = \frac{\left(2\pi\tilde{n}\frac{d}{\lambda}\cos\phi_I\right)_p}{\left(2\pi\tilde{n}\frac{d}{\lambda}\cos\phi_I\right)_s}$$

where $\widetilde{R_p}$ and $\widetilde{R_s}$ are Fresnel p-and s-polarized reflection coeffficients, Ψ is amplitude ratio, Δ is the phase shift, d is the film thickness, $\tilde{n}$ is the complex refractive index, λ is the wave length, and ϕ_I is the angle of incidence. The experimental Ψ and Δ data obtained at 50, 60, and 70° for the FL-MoS_2 sample is shown in figure 5 (dashed black). To extract the optical constants, the data was fitted (red) to an emphirical four-layer heterostructure model containing semi-infinite Si, a native SiO_2 (~2 nm) layer, BN, and MoS_2. The MoS_2 layer was modeled using a series of Kramer–Kronig consistent Tauc–Lorentz (T–L) oscillators [31]. For the fit shown in figure 5, a thickness of 2.6 nm was obtained (see table S4 for more details on fit). The data for all angles could be fit using the same model and thickness values.

In figure 6 we plot the real and imaginary part of the complex refractive index (n and k) for the FL-MoS_2 sample. The calculated ab-plane n and k values for MoS_2 layers of different thicknesses is shown as a guide and to help identify prominent optical transitions. As is clear from a casual inspection, the best agreement with our experimental refractive index value is with the calculated four-layer data (figure 6(a)). The strong features centered at 1.87 and 2.52 eV in the experimental refractive index is very close to the theoretical maxima at 1.94

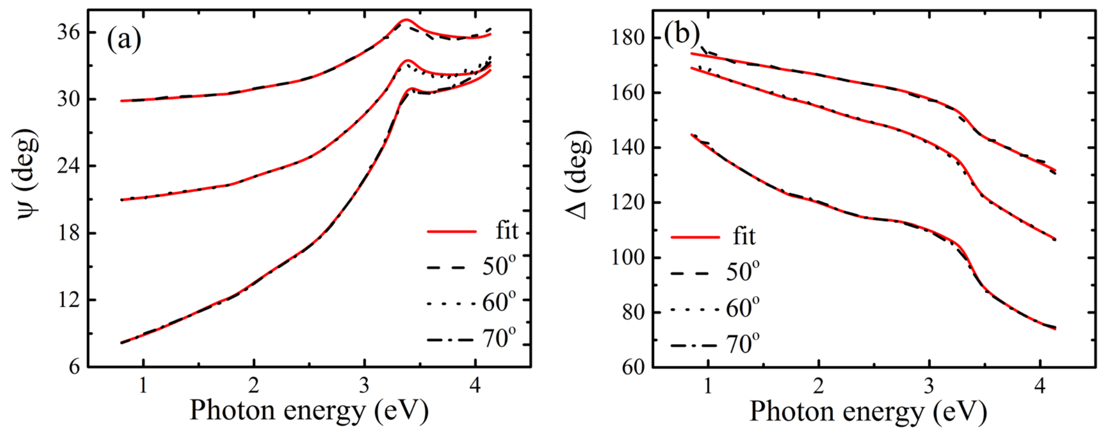

Figure 5. (a) Experimental and fitted Psi (Ψ) and (b) delta (Δ) for the FL-MoS_2 sample for incidenct angle of 50, 60, 70°. Fit of these data provided a thickness of 2.6 nm.

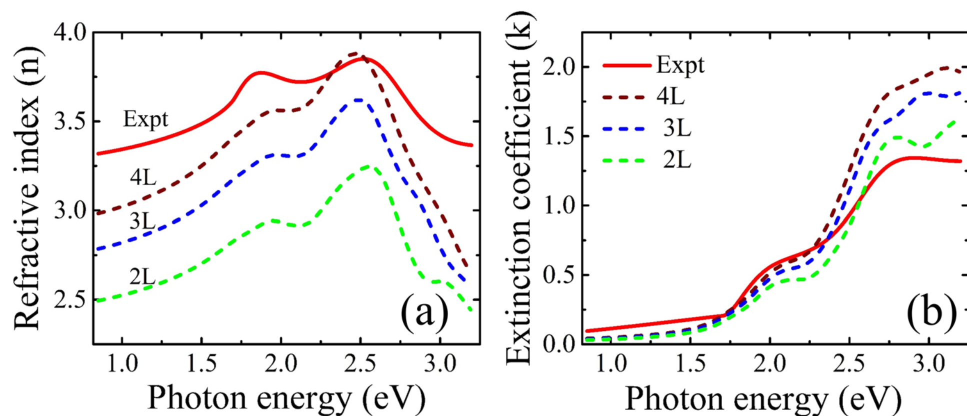

Figure 6. Real (a) and imaginary (b) part of complex refractive index. Red solid curve: experimental spectrum of the FL-MoS_2 sample; dashed curve: theoretical *a–b* plane data for 2, 3, and 4 layer MoS_2.

and 2.56 eV respectively, as highlighted. Numerous works have identified these transitions as *A*/*B* peak and *C* peak [32, 33]; *A* and *B* peaks are related to the spin–orbit split valance electrons directly transit to the VB minimum at *K* (*K*′) points. *C* peak is identified as the electron transition from valance band to conduction band at the wave vectors lie in between Gamma and *K* points. The latter is identified as a result from the band nesting effect [34, 35]. Results from our *ab initio* DFT calculations without considering the excitonic effects correctly identifies the major peaks in the experimental optical spectra [20, 32, 33]. Likewise, the features in the extinction coefficient match between theory and experiment very well. The variation of the experimental optical constants with thickness and annealing are shown and discussed in figures S5–S7.

We have further studied the electrical properties of the MoS_2/BN heterostructures. Current–voltage (*I*–*V*) measurements with two probe and four probe configurations were measured on the deposited films. For the two-probe measurements Chromium (Cr) and Gold (Au) contact pads were deposited using thermal evaporation through a metal shadow mask, and standard lithography process was followed in order to deposit four contacts using Titanium (Ti) and Gold (Au). For the two-probe measurements samples were mounted on the chip holder inside the closed cycle Helium cryostat (Janis Model # SHI-4-1) and were pumped down to high vacuum level (~10^{-6} Torr) before performing the electrical measurements. The four-probe measurements were performed under ambient conditions. Room temperature current voltage (*I*–*V*) measurements were performed using Keithley source meters (2400 series). For the *I*–*V* measurements, samples were forward and reverse biased by applying ±1 V between the contacting electrodes. It is well known that any metal semiconductor junction give rise to Schottky barrier and it is very difficult to circumvent the Schottky barrier between the semiconducting channel and the metallic contacts. However, the linearity of *IV* curves (which is a lot more prominent at low applied voltages) signifies that within the low applied voltage regime, the contacts are able to replenish the charge carriers efficiently when they are drawn out from the material under an applied electric field. Under such conditions we can assume that the contacts are 'behaving' as 'ohmic' rather than blocking or injecting.

Figure 7(a) shows the *I*–*V* curves of both the few-layer MoS_2 (2 nm)/BN and many-layer MoS_2 (20 nm)/BN heterostructures. Strikingly, 2 nm MoS_2/BN devices

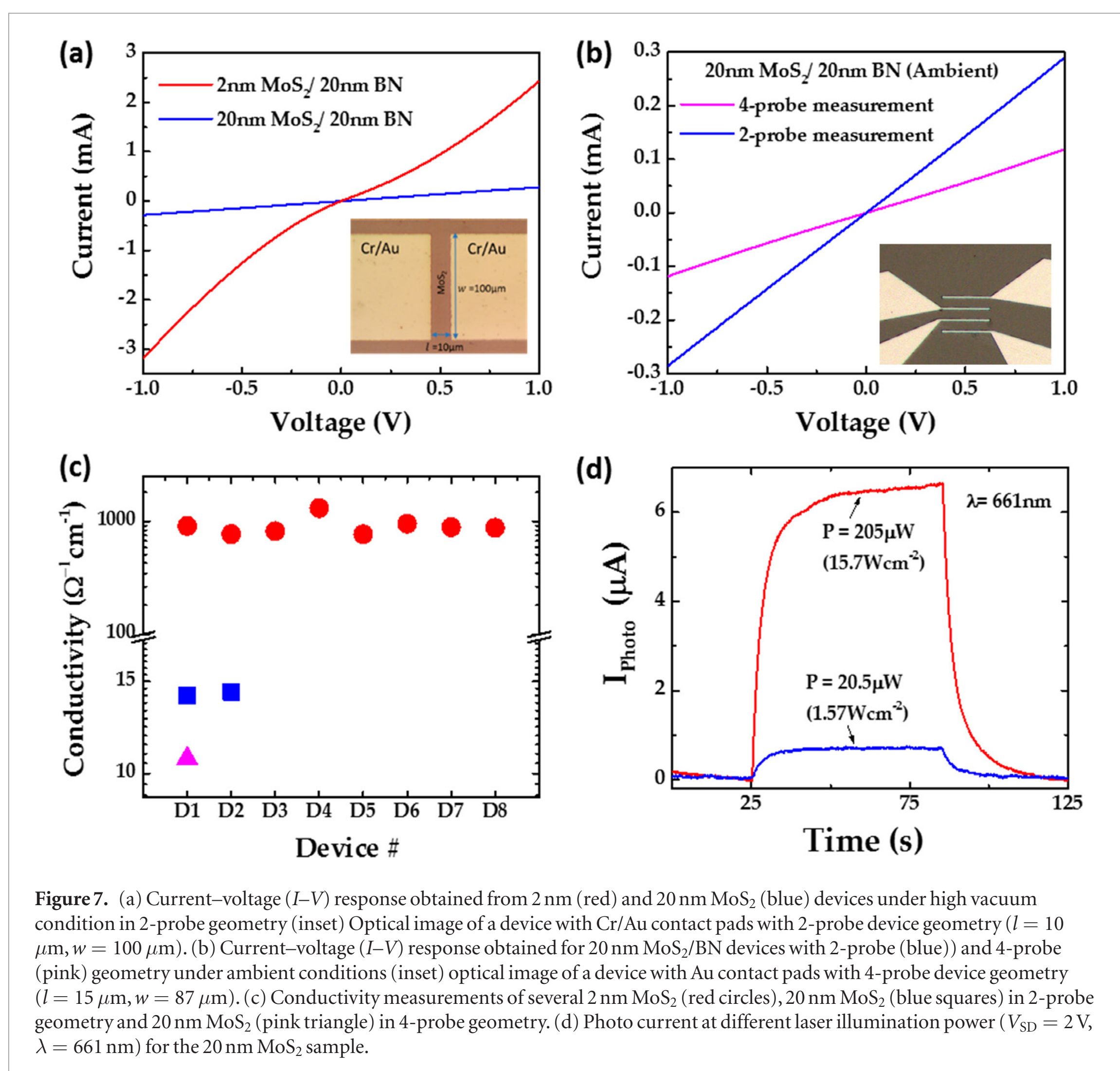

Figure 7. (a) Current–voltage (I–V) response obtained from 2 nm (red) and 20 nm MoS_2 (blue) devices under high vacuum condition in 2-probe geometry (inset) Optical image of a device with Cr/Au contact pads with 2-probe device geometry (l = 10 μm, w = 100 μm). (b) Current–voltage (I–V) response obtained for 20 nm MoS_2/BN devices with 2-probe (blue)) and 4-probe (pink) geometry under ambient conditions (inset) optical image of a device with Au contact pads with 4-probe device geometry (l = 15 μm, w = 87 μm). (c) Conductivity measurements of several 2 nm MoS_2 (red circles), 20 nm MoS_2 (blue squares) in 2-probe geometry and 20 nm MoS_2 (pink triangle) in 4-probe geometry. (d) Photo current at different laser illumination power (V_{SD} = 2 V, λ = 661 nm) for the 20 nm MoS_2 sample.

shows lower resistance (~500 Ω) than the 20 nm MoS_2/BN devices (~3.5 kΩ). In figure 7(b) a comparison of the I–V measurement on 20 nm MoS_2 measured with two point contact and four point contact is shown. Further we found the conductivity of several devices for these heterostructures. Conductivity (σ) is defined as $\sigma = l/R \cdot w \cdot t$, where l is the length between two electrode pads, w is the width of an electrode, t is the height of the MoS_2 layers and R is the measured resistance of the heterostructure devices. We found that conductivity of 2 nm MoS_2/BN heterostructure is ~2 orders higher than the 20 nm MoS_2/BN heterostructure (figure 7(c)). Also the conductivity of both of these heterostructures were several orders higher than the bulk like MoS_2 (~10^{-8} Ω^{-1} cm^{-1}) [36]. Here we would like to note that the measured conductivity with two point contact and four point contact on 20 nm MoS_2/BN device are of similar order. This is indicative of the fact that the two point measurements which were measure using larger contact pad, perhaps provides less contact resistance and hence is similar to the four point measurement where the four point geometry minimizes the contact resistance.

In the past several other groups have investigated the electrical properties of MoS_2 grown or obtained using several other techniques. For example, linear conductivity (σ') of mechanically exfoliated MoS_2 devices [37] and CVD grown MoS_2 [38] devices are indicated in table 1 where σ' is defined as $\sigma' = l/R \cdot w$. To compare with the literature we also calculated the linear conductivity of sputter deposited MoS_2 devices. As indicated in the table 1, σ' of sputter deposited MoS_2 devices are several orders higher than the mechanically exfoliated MoS_2 devices as well as CVD grown MoS_2 devices.

Here we note that the increased conductivity of few-layer films (figure 7(c) and table 1) seems contrary to the scaling behavior observed in conventional (3D) systems. First of all, in order to confirm that the conductivity in our samples is indeed from the MoS_2 layer, and not leaking from the conducting p-doped Si substrate beneath the 20 nm a-BN buffer layer we have conducted additional photo-current measurements on a 20 nm BN layer deposited on silicon substrate (see supplementary figure S8). As the figure indicates, the response of bare BN devices on Si is insensitive to incident light. We therefore found no evidence of substrate-assisted photo-conduction. This also supports the conclusion that the substrate cannot explain increase of conductivity in few-layer samples.

Table 1. Linear conductivity values of MoS_2 devices developed by different techniques.

Device	Thickness	Linear conductivity (Ω^{-1})	Reference
Mechanically exfoliated MoS_2	1 layer	~1×10^{-8}	[37]
	3 layers	~2.5×10^{-7}	[37]
CVD grown MoS_2	1–4 layers	~3.52×10^{-5}–6.85×10^{-5}	[38]
Sputter deposited MoS_2	2 nm (2-probe vac.)	~1.8×10^{-4}	This work
	20 nm (2-probe vac.)	~2.82×10^{-5}	This work
	20 nm (2-probe amb.)	~2.86×10^{-5}	This work
	20 nm (4-probe amb.)	~2.00×10^{-5}	This work

We can also put forward a few explanations as to why the enhanced conductivity of few-layer MoS_2 is reasonable. Firstly, Raman and XRD characterization (figures 3 and 4) clearly indicates that sputter-deposited many-layer films are more disordered compared to few-layer films that can explain increased conductivity. Secondly, there is also literature evidence supporting inverse-thickness scaling behavior in TMD thin films [39] which is also consistent with our results. Additionally, it is also well-documented that structural modification from 2H to 1T polytype within the MoS_2 layer can lead to metallic behavior [40], [41]. Therefore, all such evidence taken together clearly dispels the notion that conductivity is not necessarily more in case of thicker films.

In order to gauge the potential application of these films we have performed preliminary photoconductivity measurement of the 20 nm MoS_2/BN device with four-point contact (figure 7(d)). Room temperature photo switching behavior of the 20 nm MoS_2/BN devices were investigated by illuminating a $\lambda = 661$ nm laser light source with two different illumination intensities. 2 V bias voltage was applied in-between source and drain terminals ($V_{SD} = 2V$). In order to calculate the photo current, current passing through the device without light illumination (dark current; I_d) and with light illumination (illuminated current; I_{ill}) was recorded. The laser was switched on and off for about 60s at a constant intensity. This sequence was followed for 1.57 Wcm^{-2} and 15.7 W cm^{-2} laser intensities. The photo current (I_{ph}) at a particular intensity was calculated by using the equation $I_{ph} = I_{ill} - I_d$. The photo switching behavior at two different laser intensities are shown in figure 7(d). Despite the fact that photocurrent of higher laser intensity was an order higher than the photocurrent of lower laser intensity, responsivity (R) values were remained to be around ~31 mA W^{-1} for both the laser intensities. Responsivity is one of the important performance parameter of photoactive materials, is defined as the ratio of the I_{ph} and the laser illumination intensity (P_{light}). The responsivity data obtained is compared with photo response of other MoS_2 based materials (see table S6 in supplementary information). We note that the R values of the MoS_2/BN in some cases are higher than the R values of single/few layer MoS_2 devices at similar growth/measurement condition. These preliminary measurements indicate the possible use of these films in various large area opto-electronic applications.

4. Conclusion

In conclusion, we have successfully grown and investigated the structural, optical, and transport properties of few-layer MoS_2 (down to 4 monolayers) film grown on amorphous boron nitride buffered silicon substrates. A room or low temperature growth followed by post deposition annealing at a higher temperature provides the best quality MoS_2 layer with sharp interfaces. Growth of ordered few-layer crystalline MoS_2 is confirmed by x-ray, Raman spectroscopy, and ellipsometry measurements. Furthermore, the few-layers films show lower disorder compared to many-layer films. Optical properties of the MoS_2 few-layer is shown to be in very good agreement with band structure calculations. Transport measurements point to the conclusion that few-layer MoS_2 films have better conductivity than many-layer sputtered films, and compare favorably with other large-area growth methods such as CVD. Further, we have also recorded significant photo responsive behavior of these films. This has interesting and positive implications for device applications for large-area TMD films grown using sputtering.

Acknowledgments

DM would like to thank startup funds at Southern Illinois University and ST would like to acknowledge the support provided by the US Army Research Office through a MURI grant # W911NF-11-1-0362. We acknowledge the computer facilities provided by Southern Illinois University which were partly funded by National Science Foundation Awards 0721623 and 1032778. KK would like to thank for the support provided by the Academy of Finland (project Suplacat). The spectroscopic ellipsometry data shown here was carried out in the Frederick Seitz Materials Research Laboratory Central Research Facilities, University of Illinois. DM would like to acknowledge Dr Julio Soares for his help and guidance with Ellipsometry and Raman measurements.

References

[1] Neto A H C, Guinea F, Peres N M, Novoselov K S and Geim A K 2009 The electronic properties of graphene *Rev. Mod. Phys.* **81** 109

[2] Geim A K and Novoselov K S 2007 The rise of graphene *Nat. Mater.* **6** 183–91

[3] Miro P, Audiffred M and Heine T 2014 An atlas of two-dimensional materials *Chem. Soc. Rev.* **43** 6537–54

[4] Kuc A 2014 Low-dimensional transition-metal dichalcogenides *R. Soc. Chem.* **11** 1–29

[5] Fiori G, Bonaccorso F, Iannaccone G, Palacios T, Neumaier D, Seabaugh A, Banerjee S K and Colombo L 2014 Electronics based on two-dimensional materials *Nat. Nanotechnol.* **9** 768–79

[6] Wang Q H, Kalantar-Zadeh K, Kis A, Coleman J M and Strano M S 2012 Electronics and optoelectronics of two-dimensional transition metal dichalcogenides *Nat. Nanotechnol.* **7** 699–712

[7] Kang K, Xie S, Lujie H, Yimo H, Huang P Y, Mak K F, Kim C J, Muller D and Park J 2015 High-mobility three-atom-thick semiconducting films with wafer-scale homogeneity *Nature* **520** 656–60

[8] Zeng H, Dai J, Yao W, Xiao D and Cui X 2012 Valley polarization in MoS_2 monolayers by optical pumping *Nat. Nanotechnol.* **7** 490–3

[9] Mak K F, He K, Shan J and Heinz T F 2012 Control of valley polarization in monolayer MoS_2 by optical helicity *Nat. Nanotechnol.* **7** 494–8

[10] Mak K F, Lee C, Hone J, Shan J and Heinz T F 2010 Atomically thin MoS_2: a new direct-gap semiconductor *Phys. Rev. Lett.* **105** 136805

[11] Tongay S, Zhou J, Ataca C, Lo K, Matthews T S, Li J, Grossman J C and Wu J 2012 Thermally driven crossover from indirect toward direct bandgap in 2D Semiconductors: $MoSe_2$ versus MoS_2 *Nano Lett.* **12** 5576–80

[12] Zhao W, Ghorannevis Z, Chu L, Toh M, Kloc C, Tan P H and Eda G 2013 Evolution of electronic structure in atomically thin sheets of WS_2 and WSe_2 *ACS Nano* **7** 791–7

[13] Radisavljevic B, Radenovic A, Brivio J, Giacometti V and Kis A 2011 Single-layer MoS_2 transistors *Nat. Nanotechnol.* **6** 147–50

[14] Lee H S, Min S W, Chang Y G, Park M K, Nam T, Kim H, Kim J H, Ryu S and Im S 2012 MoS_2 nanosheet phototransistors with thickness-modulated optical energy gap *Nano Lett.* **12** 3695–700

[15] Yin Z, Li H, Li H, Jiang L, Shi Y, Sun Y, Lu G, Zhang Q, Chen X and Zhang H 2012 Single-layer MoS_2 phototransistors *ACS Nano* **6** 74–80

[16] Bertolazzi S, Krasnozhon D and Kis A 2013 Nonvolatile memory cells based on MoS_2/graphene heterostructures *ACS Nano* **7** 3246–52

[17] Wang H *et al* 2012 Integrated circuits based on bilayer MoS_2 transistors *Nano Lett.* **12** 4674–80

[18] Lee Y *et al* 2012 Synthesis of large-area MoS_2 atomic layers with chemical vapor deposition *Adv. Mater.* **24** 2320–5

[19] Liu Z *et al* 2014 Strain and structure heterogeneity in MoS_2 atomic layers grown by chemical vapour deposition *Nat. Commun.* **5** 5246

[20] Yim C, O'Brien M, McEvoy N, Winters S, Mirza I, Lunney J G and Duesberg G S 2014 Investigation of the optical properties of MoS_2 thin films using spectroscopic ellipsometry *Appl. Phys. Lett.* **104** 103114

[21] Seigel G, Subbaiah Y V, Prestgard M C and Tiwari A 2015 Growth of centimeter-scale atomically thin MoS_2 films by pulsed laser deposition *APL Mater.* **3** 056103

[22] Serrao C R *et al* 2015 Highly crystalline MoS_2 thin films grown by pulsed laser deposition *Appl. Phys. Lett.* **106** 052101

[23] Ho Y *et al* 2015 Layered MoS_2 grown on c-sapphire by pulsed laser deposition *Phys. Status Solidi* **9** 187–91

[24] Tao J, Chai J, Lu X, Wong L, Wong T, Pan J, Xiong Q, Chi D and Wang S 2015 Growth of wafer-scale MoS_2 monolayer by magnetron sputtering *Nanoscale* **7** 2497–503

[25] Buscema M, Steele G A, Van der Zant H J and Castellanos-Gomez A 2014 The effect of the substrate on the Raman and photoluminescence emission of single-layer MoS_2 *Nano Res.* **7** 561

[26] Lien D H *et al* 2015 Engineering light outcoupling in 2D materials *Nano Lett.* **15** 356

[27] Man M K L *et al* 2016 Protecting the properties of monolayer MoS_2 on silicon based substrates with an atomically thin buffer *Sci. Rep.* **6** 20890

[28] Wasala M *et al* 2016 Effect of underlying boron nitride thickness on photocurrent response in molybdenum disulfide—boron nitride heterostructures *J. Mater. Res.* **31** 893

[29] Bjorck M and Andersson G 2007 GenX: an extensible x-ray reflectivity refinement program utilizing differential evolution *J. Appl. Cryst.* **40** 1174–8

[30] Parratt L G 1954 Surface studies of solids by total reflection of x-rays *Phys. Rev.* **95** 359

[31] Jellison G E and Modine F A 1996 Parameterization of the optical functions of amorphous materials in the interband region *Appl. Phys. Lett.* **69** 371–3

[32] Yu Y *et al* 2015 Exciton-dominated dielectric function of atomically thin MoS_2 films *Sci. Rep.* **5** 16996

[33] Li W *et al* 2014 Broadband optical properties of large-area monolayer CVD molybdenum disulfide *Phys. Rev.* B **90** 195434

[34] Kozawa D *et al* 2014 Photocarrier relaxation pathway in two-dimensional semiconducting transition metal dichalcogenides *Nat. Commun.* **5** 4543

[35] Carvalho A, Ribeiro R M and Neto A H C 2013 Band nesting and the optical response of two-dimensional semiconducting transition metal dichalcogenides *Phys. Rev.* B **88** 115205

[36] Cunningham G, Lotya M, McEvoy N, Duesberg G S, Van der Schoot P and Coleman J N 2012 Percolation scaling in composites of exfoliated MoS_2 filled with nanotubes and graphene *Nanoscale* **4** 6260

[37] Ghatak S, Pal A N and Ghosh A 2011 Nature of electronic states in atomically thin MoS_2 field-effect transistors *ACS Nano* **5** 7707

[38] Zhan Y, Liu Z, Najmaei S, Ajayan P M and Lou J 2012 Large-area vapor-phase growth and characterization of MoS_2 atomic layers on a SiO_2 substrate *Small* **8** 966

[39] Chen R-S, Tang C-C and Huang Y-S 2014 Thickness-dependent electrical conductivities and ohmic contacts in transition metal dichalcogenides multilayers *Nanotechnology* **25** 415706

[40] Duerloo K-A N, Li Y and Reed E J 2014 Structural phase transitions in two-dimensional Mo- and W-dichalcogenide monolayers *Nat. Commun.* **5** 4214

[41] Wypych F and Schollhorn R 1992 1T-MoS_2 a new metallic modification of molybdenum disulfide *J. Chem. Soc. Chem. Commun.* **19** 1386